Journal of Power Sources 196 (2011) 7860–7867

Contents lists available at ScienceDirect

Journal of Power Sources

journal homepage: www.elsevier.com/locate/jpowsour

A study on charge storage mechanism of α-MnO_2 by occupying tunnels with metal cations (Ba^{2+}, K^+)

Dengyun Zhai [a,b], Baohua Li [a], Chengjun Xu [a], Hongda Du [a], Yanbing He [a], Chunguang Wei [a,b], Feiyu Kang [a,b,*]

[a] Advanced Materials Institute, Graduate School at Shenzhen, Tsinghua University, Shenzhen City, Guangdong Province 518055, China
[b] State Key Laboratory of New Ceramics and Fine Processing, Department of Materials Science and Engineering, Tsinghua University, Beijing 100084, China

ARTICLE INFO

Article history:
Received 28 November 2010
Received in revised form 11 April 2011
Accepted 10 May 2011
Available online 19 May 2011

Keywords:
Manganese dioxide
Charge storage mechanism
Capacitance
Tunnel

ABSTRACT

The co-existence of two mechanisms, the surface chemisorption mechanism (SCM) and the tunnel storage mechanism (TSM), for the charge storage of MnO_2 is investigated. Sample α-MnO_2 whose tunnels (2 × 2) are almost vacant is synthesized by chemical co-precipitation technique. To verify whether the charge storage of as-prepared α-MnO_2 involves the charges based on the SCM besides the TSM, Ba^{2+} and K^+ are intercalated into the tunnels of α-MnO_2 by refluxing and samples Ba-MnO_2 and K-MnO_2 are obtained, respectively. By powder X-ray diffraction, ICP and the extraction test, it is confirmed that Ba^{2+} and K^+ occupy the tunnels and are difficult to remove. By electrochemical analyses, we have found that the charge storage of Ba-MnO_2 and K-MnO_2 basically depends on the SCM, as Ba^{2+} and K^+ stabilized in the tunnels in advance block the intercalation/deintercalation of cations from the electrolyte. Thus, it can be inferred that for α-MnO_2 two mechanisms contribute to the charge storage. The contributions of α-MnO_2's mechanisms are estimated. The charges based on the TSM predominantly account for 81.2–89.9% of the total charges. The charges on the SCM may contribute to 7.9–16.8% and are not negligible. The charges from double-layer capacitance may be negligible, since it is only 1.1–4.1%.

1. Introduction

Electrochemical capacitors (ECs), which can store much more energy than conventional capacitors and offer much large power density than batteries, have been studied extensively [1,2]. Their applications include the backup or auxiliary power sources in electric vehicles and other renewable energy devices. The active materials used in ECs can be categorized into: (i) carbons based on the electrostatic interactions between the electrode and electrolyte [1,3,4], (ii) conducting polymers [5] and (iii) metal oxides which form pseudo-capacitance from the surface or bulk redox reaction [2,6,7]. Though ruthenium oxide presents the highest specific capacitance among all the metal oxides [7], its commercial application is limited by the high-cost and environment harmfulness. Lee and Goodenough [8] first reported the ideal capacitive behavior of manganese dioxide (MnO_2) in mild solutions. As MnO_2 is low-cost, nontoxic and abundant in raw materials, more studies [9–12] have focused on MnO_2 as an attractive alternative for ruthenium oxide in ECs.

The electrochemical characteristics of MnO_2 are affected by its physicochemical properties, such as particle size, surface area, morphology, crystalline structure, etc. Nowadays, MnO_2 with different crystalline structures have been prepared with their properties investigated [2,10,11]. The variety of MnO_2's structure derives from only one basic structural unit, MnO_6 octahedron. The assembling of MnO_6 units enables the formation of one-dimensional (1D), two-dimensional (2D), or three-dimensional (3D) tunnels, corresponding to the crystallographic structures shown in Fig. 1. The different structures described by the size of their tunnel are determined by the number of octahedral subunits ($n \times m$). To improve the pseudo-capacitive performance of MnO_2, the charge storage mechanism is investigated intensively. It is known that the specific capacitance of different MnO_2 is basically dependent on the surface and bulk faradic reactions [10,11]. The capacitance of MnO_2 is also affected by the species and concentrations of the alkaline metal cations in the electrolytes, as well as by the pH value. To demonstrate these phenomena, a mechanism based on the surface chemisorption mechanism (SCM) of metal cations on the surface of MnO_2 was initially proposed. The redox reaction equation of the SCM can be described by:

$$(MnO_2)_{surface} + M^+ + e^- \leftrightarrow (MnO_2{}^-M^+)_{surface} \quad (1)$$

where M^+ is the alkaline metal cations (Li^+, Na^+, or K^+) or protons. However, the experiments showed that some MnO_2 materials have much higher specific capacitance than the theoretical value based on the SCM that faradic charge storage was limited solely to the

* Corresponding author. Tel.: +86 755 2603 6118; fax: +86 755 2603 6118.
E-mail address: fykang@tsinghua.edu.cn (F. Kang).

0378-7753/$ – see front matter © 2011 Elsevier B.V. All rights reserved.
doi:10.1016/j.jpowsour.2011.05.015

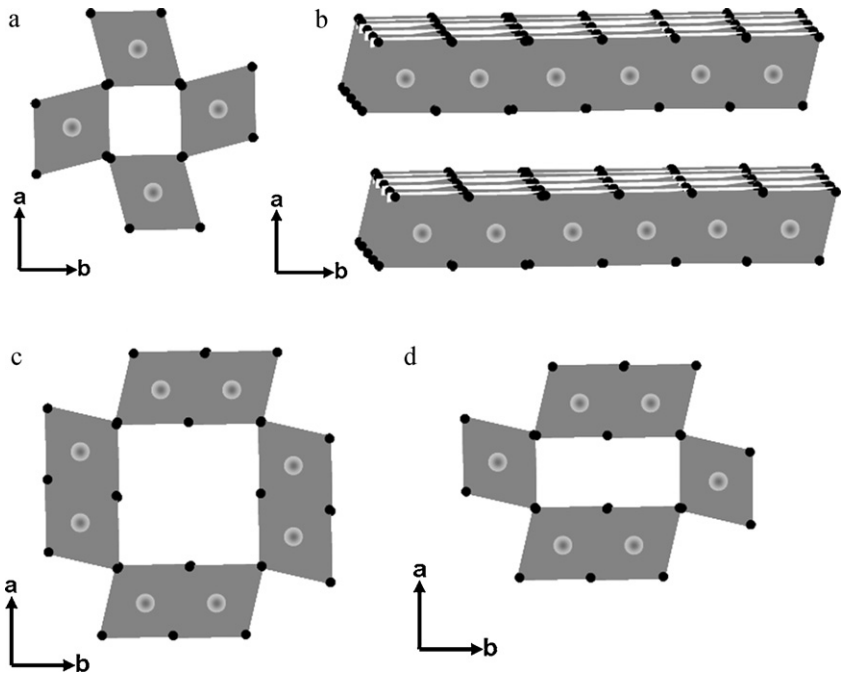

Fig. 1. Crystallographic structures of MnO_2: (a) pyrolusite β-MnO_2 (1 × 1), (b) birnessite δ-MnO_2 (1 × ∞), (c) hollandite α-MnO_2 (2 × 2), and (d) ramsdellite γ-MnO_2 (1 × 2).

surface of MnO_2 [2,11]. To account for this discrepancy, a tunnel storage mechanism (TSM) was proposed. The redox process of the TSM is mainly governed by the insertion/deinsertion of alkaline metal cations and protons of the electrolyte into/from the structural tunnel of MnO_2, which is expressed by

$$MnO_2 + xM^+ + xe^- \leftrightarrow M_xMnO_2 \quad (2)$$

where M^+ is the alkaline metal cations (Li^+, Na^+, or K^+) or protons. Toupin et al. [13] used ex situ X-ray photoelectron spectroscopy (XPS) to demonstrate the existence of the TSM. Meanwhile, a reversible expansion and shrinkage in lattice spacing of the oxide during charge transfer at manganese sites upon reduction/oxidation of MnO_2 was also demonstrated by in situ synchrotron X-ray diffraction [14]. It indicated that the insertion of cations into the tunnel occurs in the charge storage process of MnO_2.

Up to now, most researchers accepted the TSM as the main mechanism that contributes to the specific capacitance of MnO_2. However, a few researchers [10,15] still supposed that in addition to the TSM, the effect of the SCM on the electrochemical performance of MnO_2 may not be negligible. It remains unclear how much role the SCM plays on the specific capacitance of MnO_2.

In this paper, from the viewpoint of electrochemical analysis we will investigate whether the two mechanisms can both contribute to the charge storage of MnO_2, and then estimate, if both contribute, what the proportion of their contributions is. An experiment was conducted for the above aims. According to the TSM, when most of the MnO_2 tunnels are unoccupied, the alkaline metal cations and protons can insert into/deinsert from the tunnels during the redox process. If the MnO_2 tunnels are pre-filled with the metal cations that cannot be easily removed, the intercalation/deintercalation of cations in the electrolyte cannot occur. Then the TSM has no effect on the specific capacitance. In this study, the electrochemical performance of MnO_2 whose their tunnels were empty or pre-filled with cations was investigated. Finally, the relative contributions of TSM and SCM to the specific capacitance were estimated.

Manganese dioxide materials possess various crystalline structures. The electrochemical characteristics of α-MnO_2 (2 × 2), whose capacitance depends distinctly on the TSM, were reported [9,16,17]. For α-MnO_2,the alkali metal ions were inserted into/extracted from the (2 × 2) tunnels by two different mechanisms: redox-type and ion-exchange-type reactions [18]. As there are the defects in the Mn sites, the lattice protons may occupy the (2 × 2) tunnel sites [19]. The metal ions can insert into the tunnels by exchanging with the protons of the tunnels. By refluxing or autoclaving the metal ions can insert into the tunnels through ion-exchange-type reaction. The exchanging process is very slow and needs several days [18]. At the same time it is difficult and time-consuming to extract the ions which have been inserted into the tunnel in advance by ion-exchange-type reaction [18,20]. The other mechanism is the redox-type reaction. It proceeds at certain voltage in a few hours or minutes and can change the valence of manganese. It indicates that two insertion/deinsertion processes have different mechanism and need different reaction time. Thus, after the metal ions have been inserted into the (2 × 2) tunnels by ion-exchange-type reaction, they can effectively block the intercalation of metal ions by redox-type reaction. The intercalation of cations (Li^+, K^+, NH_4^+, and Ba^{2+} ions) into the tunnel sites of α-MnO_2 can be accomplished by refluxing or autoclaving an acidic solution of $KMnO_4$ and Mn^{2+} [18,21,22]. The α-MnO_2 occupied by Ba^{2+} is called hollandite, and the one by K^+ is cryptomelane. The α-MnO_2, hollandite and cryptomelane have the same crystalline structure, and are known as α-MnO_2's [23]. In the present work, α-MnO_2's were synthesized and the charge storage mechanisms were investigated.

2. Experimental

2.1. Preparation of α-MnO_2's

The α-MnO_2 powder was synthesized from Mn(VII) and Mn(II) by chemical co-precipitation technique according to the following:

$$2Mn(VII) + 3Mn(II) \rightarrow 5Mn(IV) \quad (3)$$

The Mn(VII)/Mn(II) molar ration is 2:3. The 0.2 M $KMnO_4$ solution was prepared by dissolving potassium permanganate (AR, 99%) in deionized water. The 0.3 M $Mn(CH_3COO)_2$ solution was also prepared at the same way. While stirring the $Mn(CH_3COO)_2$ solution, 0.2 M $KMnO_4$ solution was added quickly. A dark brown

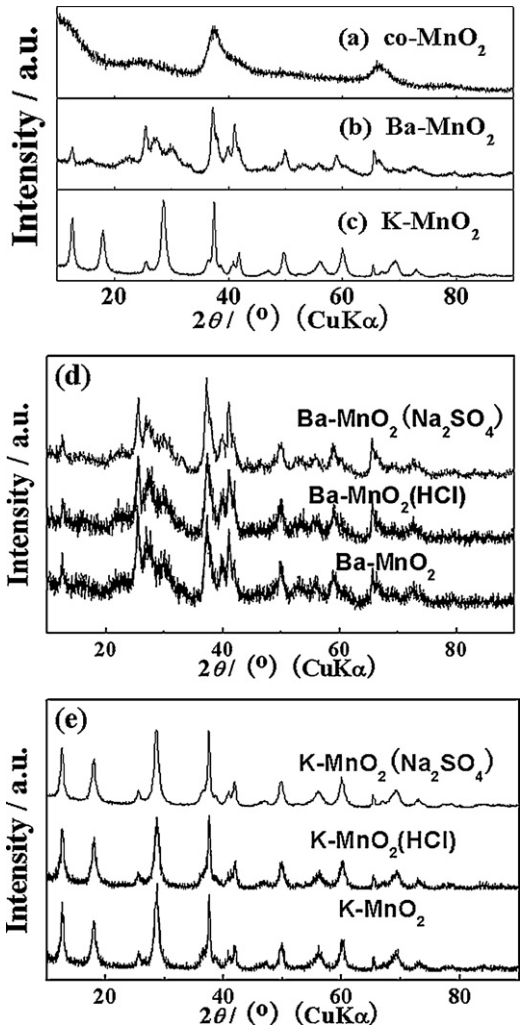

Fig. 2. XRD patterns of samples: (a) co-MnO_2, (b) Ba-MnO_2, and (c) K-MnO_2; XRD patterns of samples after the extraction test: (d) Ba-MnO_2 and (e) K-MnO_2.

precipitation was obtained. The solution was then stirred for 4 h at ambient temperature until the reaction completed. The precipitation was filtered, washed several times with deionized water, and dried at 80 °C for 24 h. The sample was denoted as co-MnO_2.

The cryptomelane powder was synthesized as follows: 100 ml of 0.2 M $KMnO_4$ solution was added to 100 ml of 0.3 M $Mn(CH_3COO)_2$ solution. At once the solution was refluxed at 100 °C for 24 h, and the product was filtered, washed with deionized water, and dried at 80 °C for 24 h. The sample was denoted as K-MnO_2. The hollandite powder was obtained as follows: 3.19 g of $Ba(CH_3COO)_2$ was added into the 100 ml of 0.3 M $Mn(CH_3COO)_2$ solution, followed by 100 ml of 0.2 M $KMnO_4$ solution. The solution was refluxed at 100 °C for 24 h, and the product was filtered, washed, and dried at 80 °C for 24 h. The sample was denoted as Ba-MnO_2.

2.2. Characterization

Powder X-ray diffraction (XRD) patterns of samples were obtained by using a TW3040/60 diffractometer (Tanalygical Company, Holland) in which Cu-Kα ($\lambda = 0.154$ nm) was used as the radiation source. Elemental compositions for manganese, potassium and barium were analyzed by inductively coupled plasma-atomic emission spectroscopy (ICP-AES, ICPS6300). The morphologies of the powder samples were examined by a Hitachi S-4800 scanning electron microscopy (SEM) and a transition electron microscope (TEM) (Jeol JEM2100F). The surface area and pore volume of the samples were determined by nitrogen adsorption at 77 K with an automated adsorption apparatus (Micromeritics ASAP 2020). The surface area was determined from the Brunauer–Emmett–Teller (BET) equation. The pore size distribution was determined by the BJH method [24] from the desorption isotherm.

2.3. Electrochemical measurement

Electrodes were prepared by mixing 70 wt% of MnO_2 powder as active material with 20 wt% acetylene black and 10 wt% polytetrafluoroethylene (PTFE). 70 mg of MnO_2 powder and 20 mg of acetylene black were first mixed and dispersed in ethanol by ultrasonic stirring for 30 min. Then the ink was dried at 80 °C for 12 h and 200 mg of PTFE aqueous solution (5 wt%) was added to form a paste. Then the paste was dried at 80 °C and a few drops of 1-methy-2-pyrrolidinone (NMP) were added to get a syrup. The syrup was rolled into thick films. The films were cut into the 1 cm × 1 cm pieces of about 3 mg, and then hot-pressed at 80 °C under 100 MPa onto a stainless steel mesh connected to a nickel wire.

Electrochemical tests were performed with a battery system VMP3 (Bio-Logic Corp., France). A piece of platinum gauze and a saturated calomel electrode (SCE) were assembled as the counter and reference electrode, respectively. 0.1 M $Ba(NO_3)_2$ and 0.1 M KNO_3 were used as the electrolytes. The cyclic voltammetry (CV) measurements were carried out at scanning rates ranging from 2 to 50 mV s^{-1}. The potential range was from 0.1 to 0.9 V versus SCE in 0.1 M $Ba(NO_3)_2$ and from 0.05 to 0.8 V versus SCE in 0.1 M KNO_3, respectively.

To examine the stability of Ba^{2+} and K^+ in the tunnel sites, the extraction test was performed as follows: 0.5 g of as-prepared Ba-MnO_2 (or K-MnO_2) was stirred separately in a 0.1 M HCl solution (200 ml) and 0.1 M Na_2SO_4 (200 ml) for 48 h and the samples were filtered, washed, and dried at 80 °C for 24 h. The resultant powders were characterized by XRD and ICP elemental analyses. The electrochemical performance was conducted on the samples.

3. Results and discussion

3.1. Characteristics

Fig. 2 shows the XRD patterns of the samples. It can be seen in Fig. 2a that a few broad peaks around $2\theta = 37.0°$ and 65.3° present to indicate the amorphous nature. The profile of peaks seems to correspond to some peaks of α-MnO_2 (JCPDS No. 44-0141) [9,12,13]. The XRD pattern of Ba-MnO_2 is shown in Fig. 2b. The profile of peaks corresponds to the crystalline phase of hollandite (JCPDS No. 78-0962), and the broadening of peaks indicates that the sample presents in partially crystalline state. Fig. 2c shows that the XRD pattern of K-MnO_2 corresponds to the cryptomelane (JCPDS No. 29-1020) [21,22]. Thus, according to the XRD data, Ba^{2+} and K^+ were inserted successfully into the tunnel (2 × 2) of α-MnO_2. From ICP elemental analyses, the K/Mn and Ba/Mn molar ratios were obtained and the chemical formulas of three samples are $K_{0.13}Mn_8O_{16}$ (co-MnO_2), $K_{1.12}Mn_8O_{16}$ (K-MnO_2) and $Ba_{1.86}Mn_8O_{16}$ (Ba-MnO_2), respectively. This indicated that most of the tunnels of co-MnO_2 were unoccupied, and Ba^{2+} and K^+ were set in the tunnels of Ba-MnO_2 and K-MnO_2, respectively.

The samples of Ba-MnO_2 and K-MnO_2 after the extraction test were characterized by XRD, as shown in Fig. 2d and e. It can be seen that there is no significant difference between XRD patterns of the samples before and after immersed in 0.1 M HCl and 0.1 M Na_2SO_4. The results of ICP also showed that the molar ratios of Ba/Mn and K/Mn decreased little after immersing. Thus, Ba^{2+} and

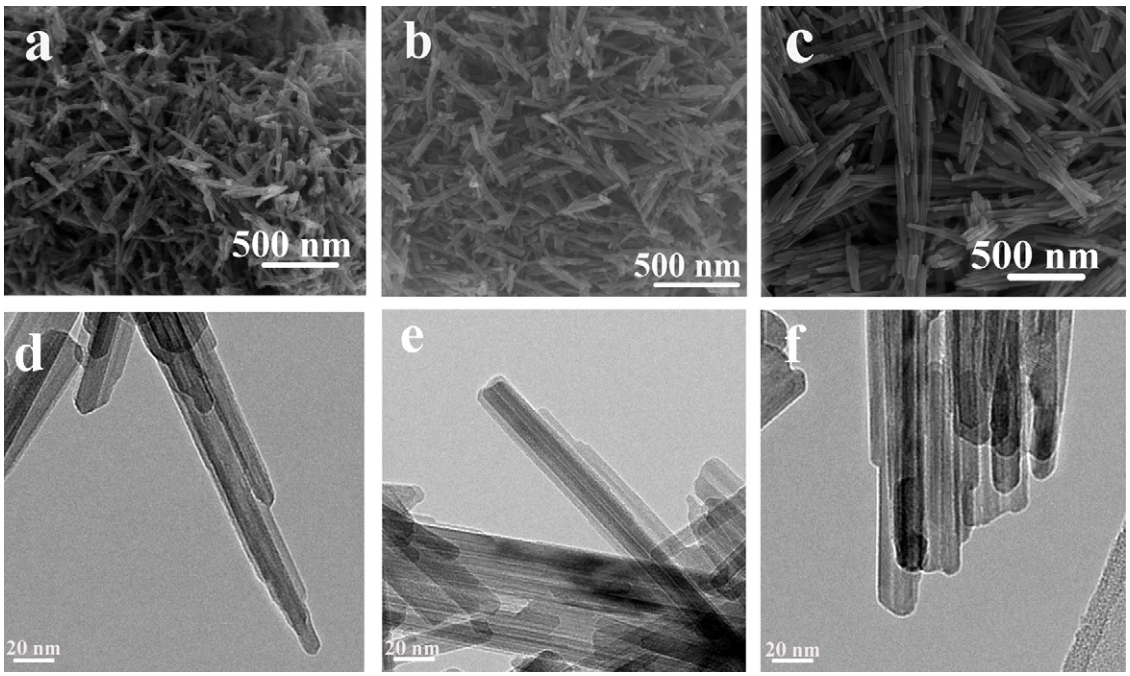

Fig. 3. SEM images of three samples: (a) co-MnO_2, (b) Ba-MnO_2 and (c) K-MnO_2; TEM images of three samples: (d) co-MnO_2, (e) Ba-MnO_2 and (f) K-MnO_2.

K^+ were inserted into the tunnels by ion-exchange-type reaction, stabilized in the tunnels and not easily removed [18,21].

The surface morphologies of three samples (co-MnO_2, Ba-MnO_2 and K-MnO_2) are shown in Fig. 3. It can be seen that all the samples have similar rod-like morphology. The diameter of nanorods is about 20 nm. Fig. 3c and f also show that the K-MnO_2 nanorods appear more in bundles. It is known that the morphology of host materials has an effect on the ion's diffusivity. The size and shape of MnO_2 particles will influence the ions' diffusivity inside the particles. The samples co-MnO_2, Ba-MnO_2 and K-MnO_2 have similar morphology, and it makes the effect of the morphology similar. The nitrogen adsorption/desorption isotherms of the samples are shown in Fig. 4. The isotherm of co-MnO_2 is typical for a mesoporous material with a hysteresis loop for relative pressure (P/P_0) range between 0.5 and 0.9, corresponding to Type IV. The isotherms of Ba-MnO_2 and K-MnO_2 show that the amount adsorbed increases sharply above 0.9 P/P_0, resembling Type III, which suggests that the multilayer adsorption process occurs inside the mesopores or macropores. The specific surface area was calculated by BET equation and the specific surface area of co-MnO_2 (226.22 $m^2\,g^{-1}$) is much larger than those of Ba-MnO_2 (80.66 $m^2\,g^{-1}$) and K-MnO_2 (56.74 $m^2\,g^{-1}$). Fig. 5 shows the pore size distribution of the three samples determined by the BJH method. The dominant peak near 5 nm is observed in the curve of co-MnO_2, and the broad peak (inset in Fig. 5) in the curve of Ba-MnO_2 and K-MnO_2 locates in the range from 40 to 80 nm. Referring to the surface morphology of co-MnO_2, which consists of the nanorods with the diameter of about 20 nm, co-MnO_2 may possess a porous structure with the pore of 4–6 nm [9], and thus the specific surface area is relatively high. As the Ba-MnO_2 and K-MnO_2 were synthesized at 100 °C, high temperature oriented the nanorods to grow to perfect status. Thus the porous structure disappeared and the nanorods piled up and formed the pores around 40–80 nm. Though the difference of the surface area between three samples is obvious, the electrochemical performance of MnO_2 depends more on the surface and bulk faradic reactions than on the surface area.

From the above characteristics including XRD pattern, ICP elemental analyses, SEM, TEM and nitrogen adsorption, three as-prepared samples have same tunnel structure (2×2) and surface morphology. The main difference among them is that Ba^{2+} and K^+

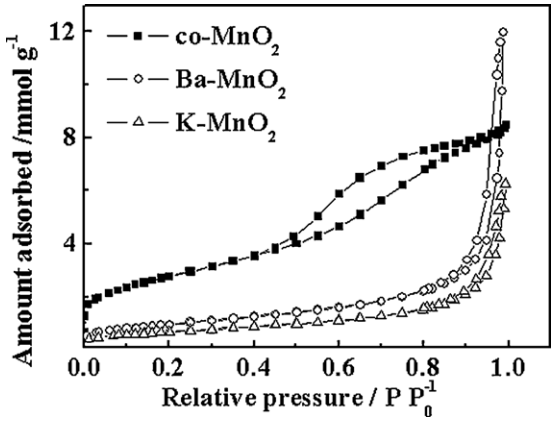

Fig. 4. Nitrogen adsorption/desorption isotherms at 77 K for co-MnO_2, Ba-MnO_2 and K-MnO_2.

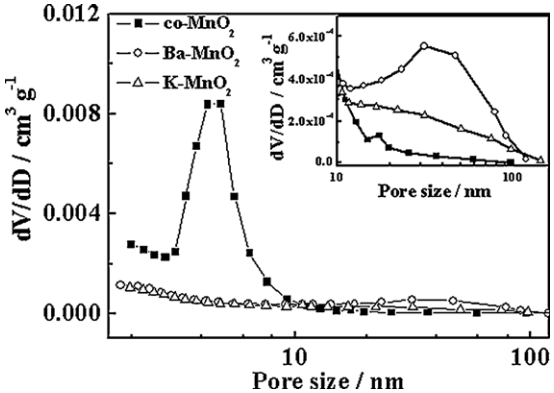

Fig. 5. The pore size distribution calculated by BJH method for co-MnO_2, Ba-MnO_2 and K-MnO_2.

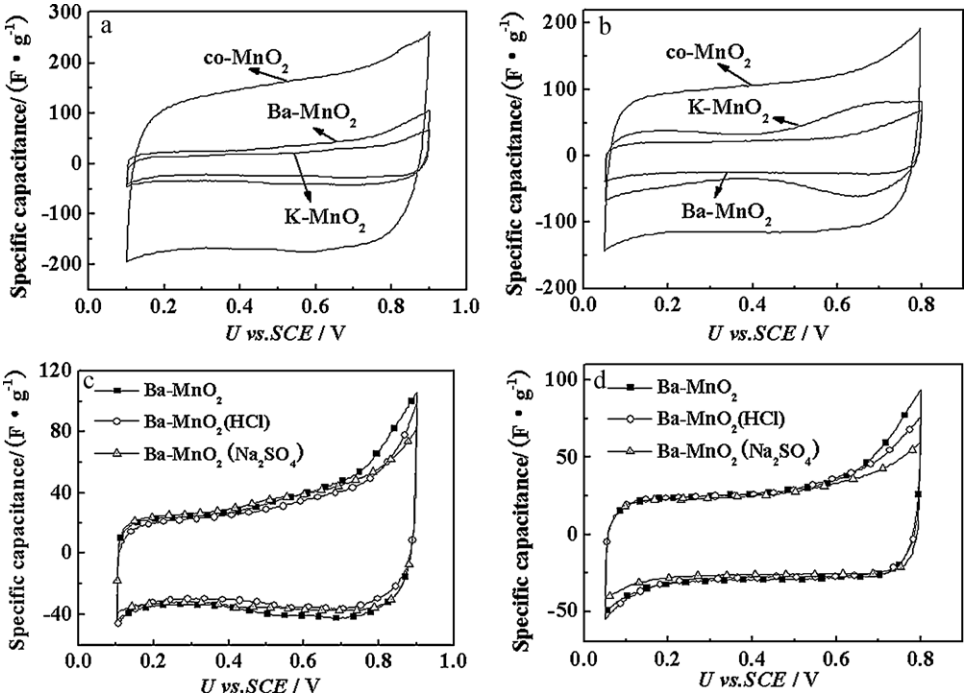

Fig. 6. Cyclic voltammograms of co-MnO_2, Ba-MnO_2 and K-MnO_2 at the scanning rate of 2 mV s^{-1} in (a) 0.1 M $Ba(NO_3)_2$ and (b) 0.1 M KNO_3; cyclic voltammograms of Ba-MnO_2 after the extraction test at the scanning rate of 2 mV s^{-1} in (c) 0.1 M $Ba(NO_3)_2$ and (d) 0.1 M KNO_3.

were filled in the tunnels (2×2) of Ba-MnO_2 and K-MnO_2, while the tunnels of co-MnO_2 were almost vacant.

3.2. Electrochemical properties

Typical CV measurements were conducted for as-prepared samples in 0.1 M $Ba(NO_3)_2$ and 0.1 M KNO_3 solutions. The potential ranges were 0.1–0.9 V and 0.05–0.8 V versus SCE, respectively, and the measurements were taken at different scanning rates from 2 to 50 mV s^{-1}.

Fig. 6 shows that the cyclic voltammetry curves of the samples at the scanning rate of 2 mV s^{-1}. The curves are relatively rectangular in shape, and the current response to voltage reversal exhibits near mirror-image, indicating a reversible reaction and ideal capacitive behavior. The electrochemical properties of Ba-MnO_2 and K-MnO_2 after the extraction test were also performed. As shown in Fig. 6c and d, CVs of Ba-MnO_2 after immersed in both solutions coincide with the ones before immersed. The CVs of K-MnO_2 after immersed are the same with the ones before immersed and not present here. As the structure and chemical component of Ba-MnO_2 and K-MnO_2 after the extraction test did not change, the electrochemical performance remained unchanged. The average specific capacitance (SC) was calculated by the general equation

$$C = \frac{Q}{\Delta E \times m} \tag{4}$$

where C is the specific capacitance, Q is the half charge obtained after integrating the voltammogram, m is the mass of the active material, and ΔE is the potential window. In 0.1 M $Ba(NO_3)_2$, the SC of co-MnO_2, Ba-MnO_2 and K-MnO_2 is 158, 36 and 24 F g^{-1}, respectively. And in 0.1 M KNO_3 the SC of three samples is 111, 26 and 44 F g^{-1}, respectively. Brousse et al. [11] summarized the electrochemical performance of MnO_2 materials for ECs and found the trend that the SC was scattered between 110 and 210 F g^{-1} for α-MnO_2 having a surface area larger than 125 m^2 g^{-1}. In the present work, the electrochemical performance of as-prepared α-MnO_2 corresponds to the above trend. The SC of co-MnO_2 in 0.1 M $Ba(NO_3)_2$ is larger than that in 0.1 M KNO_3. Xu et al. [2,17] investigated the effect of different valent cations on capacitive behavior and charge storage mechanism of α-MnO_2. When the insertion/deinsertion process of cations occurred, instead of one univalent cation, one bivalent cation (such as Ca^{2+}, Ba^{2+}) can also intercalate into the tunnel of α-MnO_2 to store two electrons, twice of the univalent cation, and more charges can be stored. Thus, the SC of as-prepared co-MnO_2 in 0.1 M $Ba(NO_3)_2$ is larger than that in 0.1 M KNO_3. This indicates that the TSM has a distinct effect on the charge storage for co-MnO_2. In both solutions, the SC of Ba-MnO_2 and K-MnO_2 is much lower than that of co-MnO_2. As the main difference between Ba/K-MnO_2 and co-MnO_2 is that the tunnels of Ba/K-MnO_2 are stabilized by Ba^{2+}/K^+, it may be supposed that the cations filled in advance may block the cations in the solution from intercalating into the tunnel. Therefore, the charge storage of Ba-MnO_2 and K-MnO_2 is not stored based on the TSM. And the SC of Ba-MnO_2 and K-MnO_2 may be attributed to the charge storage based on the SCM.

The cyclic voltammetry curves of three samples in 0.1 M $Ba(NO_3)_2$ at different scanning rates of 2–50 mV s^{-1} are shown in Fig. 7a–c for co-MnO_2, Ba-MnO_2 and K-MnO_2, respectively. With increasing the scanning rate, CVs of co-MnO_2 become distorted dramatically and CVs of Ba-MnO_2 and K-MnO_2 remain rectangular shape. For the three samples in 0.1 M KNO_3, the CVs are similar to Fig. 7 and therefore are not presented here. According to Eq. (4), the dependence of the SC calculated from CVs on scanning rate is shown in Fig. 8. In 0.1 M $Ba(NO_3)_2$, from 2 to 50 mV s^{-1} the SC of co-MnO_2 decreases sharply from 158 to 53 F g^{-1}, and the SC of Ba-MnO_2 and K-MnO_2 decreases from 36 to 30 F g^{-1} and from 24 to 20 F g^{-1}, respectively. In 0.1 M KNO_3 the SC of co-MnO_2 decreases drastically from 111 to 43 F g^{-1} and the SC of Ba-MnO_2 and K-MnO_2 decreases only by 16.5% and 18.6%, respectively.

As mentioned earlier on the charge storage mechanism of MnO_2, two mechanisms may be proposed. One is the surface chemisorption mechanism, based on adsorption/desorption of protons or cations on the MnO_2 surface. The other is the tunnel storage mechanism based on intercalation/deintercalation of protons or cations

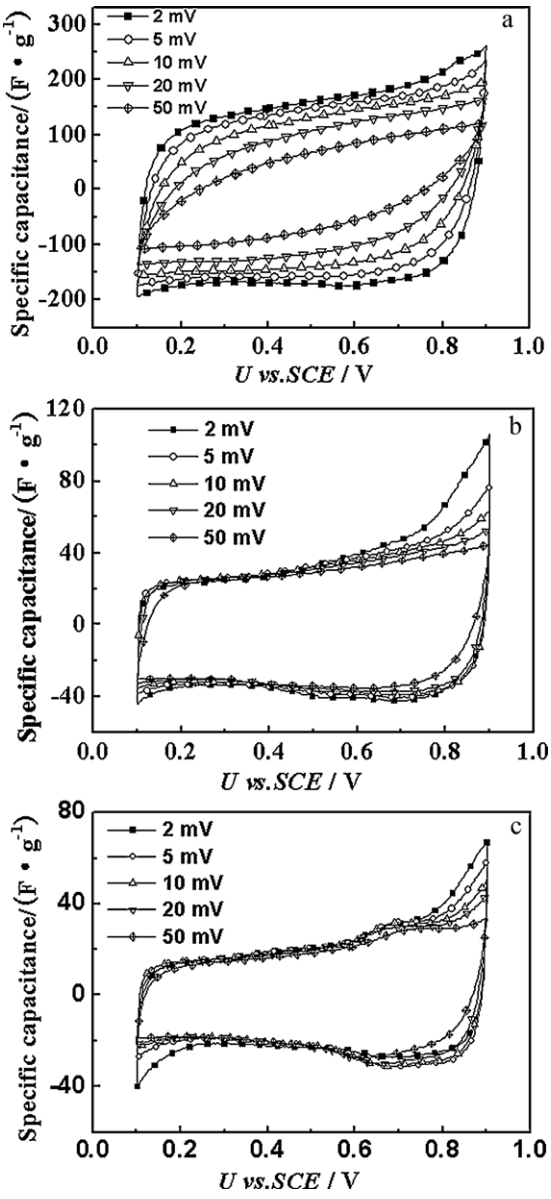

Fig. 7. Cyclic voltammograms of three samples at different scanning rates in 0.1 M $Ba(NO_3)_2$: (a) co-MnO_2, (b) Ba-MnO_2 and (c) K-MnO_2.

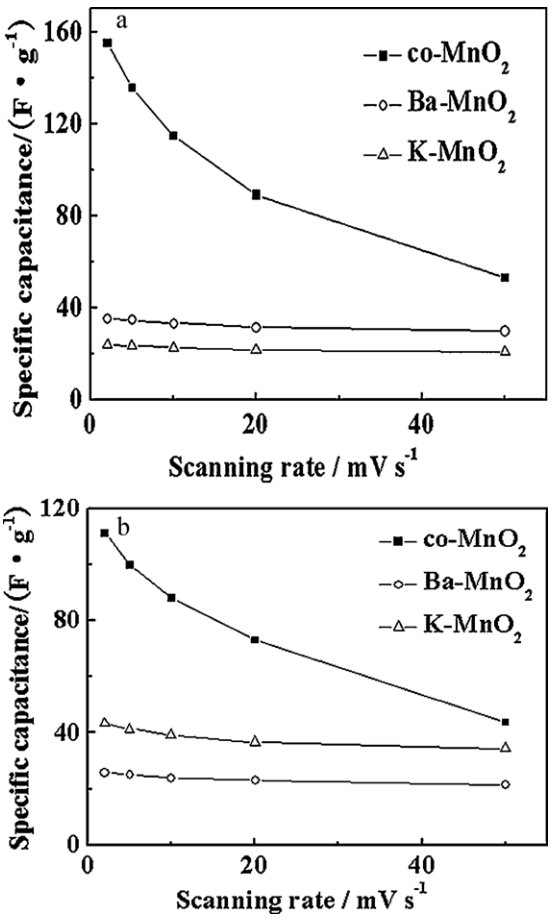

Fig. 8. The dependence of SC on scanning rate for co-MnO_2, Ba-MnO_2 and K-MnO_2 in (a) 0.1 M $Ba(NO_3)_2$ and (b) 0.1 M KNO_3.

into/from the tunnels of MnO_2. At slow scanning rate, protons or cations have enough time to arrive at the surface of MnO_2 and to insert into the tunnel of MnO_2, and thus both mechanisms are effective on the charge storage. At fast scanning rate, protons and cations may not have enough time to intercalate into the tunnels, but may be able to reach the surface, thus the charges stored from the TSM may become less and the SCM remains effective on the charge storage. Referring to Figs. 7 and 8, with increasing scanning rate the SC of co-MnO_2 decreased drastically and the SC of Ba-MnO_2 and K-MnO_2 dropped only a little. Thus, the charge storage of co-MnO_2 is probably related to the TSM, and the charge storage of Ba-MnO_2 and K-MnO_2 may mainly depend on the SCM.

Ardizzone et al. [25] firstly proposed the method to discriminate so called "inner" and "outer" charges. The whole surface of MnO_2 could be divided into "inner" surface and "outer" surface. "Inner" surface involves the micropores inside particles, tunnels piled up, etc., which is more difficult to access. And "outer" surface involves mesopores and the surface of grain, which is easily accessible for ions. At fast scanning rate, protons or cations can only arrived at the "outer" surface of MnO_2. Thus the extrapolation of q to $v = \infty$ from the q versus $v^{-1/2}$ plot gives the "outer" charge of q_0, which is the charge on the most accessible active surface. The extrapolation of q to $v = 0$ from the q^{-1} versus $v^{1/2}$ plot gives the total charge q_T, that is, the charge related to the whole active surface [9,12,26,27].

The voltammetric charges have been determined as a function of the scanning rate. The dependence of voltammetric charge q on $v^{-1/2}$ for the three samples is shown in Fig. 9a and b for 0.1 M $Ba(NO_3)_2$ and 0.1 M KNO_3 solutions, respectively. In Fig. 10a and b, the inverse of the voltammetric charge q^{-1} is plotted as a function of $v^{1/2}$. The data are linearly fitted with least square method. The estimated charges at very low and very high scanning rates in different solutions for three samples are presented in Table 1. At very low scanning rate, q_T of co-MnO_2 in 0.1 M $Ba(NO_3)_2$ is 332.22 C g^{-1}, about twice of q_T (165.29 C g^{-1}) in 0.1 M KNO_3. The results match the tunnel storage mechanism of bivalent cations proposed by Xu et al. [2,17]. In both solutions, the q_0 values of co-MnO_2 are close each other, 33.39 and 31.12 C g^{-1} in 0.1 M $Ba(NO_3)_2$

Table 1
The estimated charge density at very low and very high scanning rate in different solutions for three samples.

Solution	Sample	q_0 (C g^{-1})	q_T (C g^{-1})	q_0/q_T (%)
0.1 M $Ba(NO_3)_2$	co-MnO_2	33.39	332.22	10.0
	Ba-MnO_2	22.50	29.84	75.4
	K-MnO_2	15.89	19.84	80.1
0.1 M KNO_3	co-MnO_2	31.12	165.29	18.8
	Ba-MnO_2	15.23	20.50	74.3
	K-MnO_2	23.50	34.64	67.8

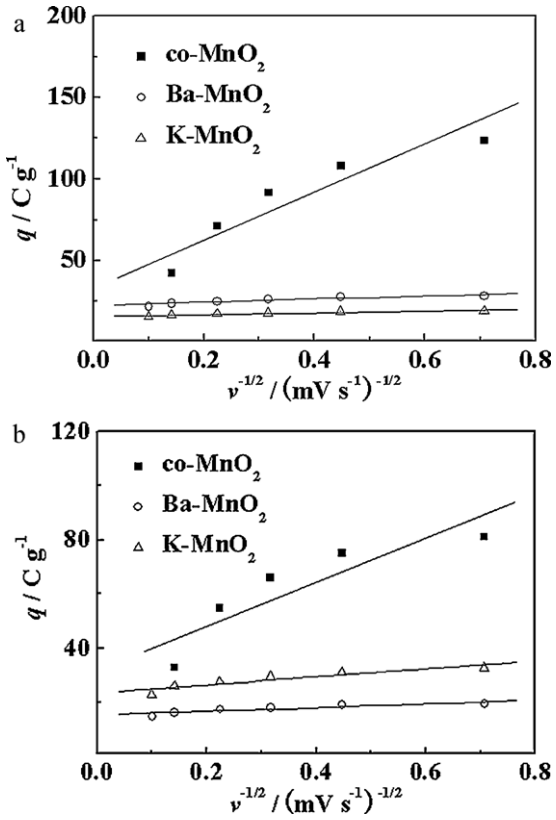

Fig. 9. Variation of the voltammetric density (q) with respect to scanning rate (v) plotted as q versus $v^{-1/2}$ for co-MnO_2, Ba-MnO_2 and K-MnO_2 in (a) 0.1 M $Ba(NO_3)_2$ and (b) 0.1 M KNO_3.

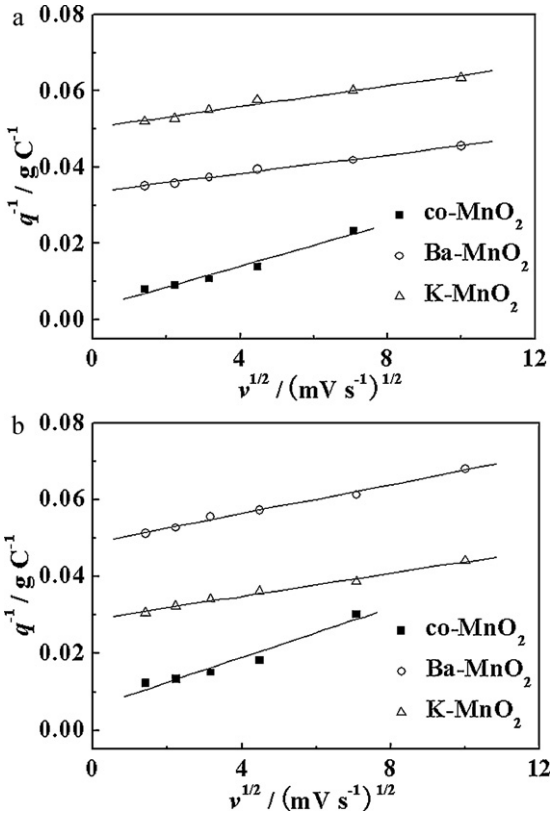

Fig. 10. Variation of the voltammetric density (q) with respect to scanning rate (v) plotted as q^{-1} versus $v^{1/2}$ for co-MnO_2, Ba-MnO_2 and K-MnO_2 in (a) 0.1 M $Ba(NO_3)_2$ and (b) 0.1 M KNO_3.

and 0.1 M KNO_3, respectively, and the values of q_0/q_T are very low, 10.0 and 18.8%, respectively. The results indicate that the charges based on the TSM predominate within the charge storage of co-MnO_2 and the charges based on the SCM account only for a small proportion of the total charges.

The q_T values of Ba-MnO_2 in both solutions are very small, only 29.84 and 20.50 C g^{-1}, respectively, and the values of q_0/q_T rise up to 75.4% and 74.3%, respectively. The same result is found for K-MnO_2. It can be deduced that as most of the tunnels of Ba-MnO_2 and K-MnO_2 were pre-occupied, the charge storage may be basically dependent on the SCM. The values of q_0 of Ba-MnO_2 in 0.1 M $Ba(NO_3)_2$ (22.50 C g^{-1}) is larger than that in 0.1 M KNO_3 (15.23 C g^{-1}); in the same way, q_0 of K-MnO_2 in 0.1 M $Ba(NO_3)_2$ (15.89 C g^{-1}) is smaller than in 0.1 M KNO_3 (23.50 C g^{-1}). That is, for Ba-MnO_2 and K-MnO_2, the contribution of the surface charge storage in the electrolyte containing same cations is higher than in the electrolyte containing hetero cations, probably because the electrolyte containing identical cations is in favor of the surface charge storage.

In a word, we can infer that for as-prepared co-MnO_2, both the TSM and SCM contributed to the charge storage and the charges based on the TSM predominate within the total charges. On the other hand, for as-prepared Ba-MnO_2 and K-MnO_2, the charge storage is basically dependent on the SCM, as most of the tunnels were occupied in advance.

Of course, for as-prepared co-MnO_2, the tunnel sites were not all vacant and the ions such as protons or K^+ occupied a small number of the tunnel sites while synthesized. The tunnels of as-prepared Ba-MnO_2 and K-MnO_2 were not fully occupied by cations [18,21]. When the redox process of co-MnO_2 occurs, a few tunnels pre-occupied by ions cannot store the charges, and the SC and q from the experiments are expected to be lower than the theoretical value. At the same time, a few vacant tunnels for Ba-MnO_2 and K-MnO_2 can be intercalated/deintercalated by the cations in the electrolyte. However, in the present work the obtained data was good enough for estimating the contribution of the SCM and TSM approximately.

When we estimated the contribution of the SCM and TSM of the samples approximately, the effect of the surface area should be involved. The surface area may have the effect on the double-layer capacitance based on the electrostatic interactions between the electrode and electrolyte, as well as on the SCM. For Ba-MnO_2 and K-MnO_2 with broad distribution between 40 and 80 nm, the macropore volume is the only channel that the electrolyte enters into the mesopores and micropores, and stores few charges based on double-layer effect [28,29]. Thus, q_0 of Ba-MnO_2 and K-MnO_2 is attributed to the SCM. q_0 of Ba-MnO_2 in 0.1 M $Ba(NO_3)_2$ (22.50 C g^{-1}) was very closed to q_0 of K-MnO_2 in 0.1 M KNO_3 (23.50 C g^{-1}), which illustrate that the optimal charges based on the SCM may be about 23 C g^{-1} in both solutions. For co-MnO_2 with single narrow mesoporous distribution of 4–6 nm, double-layer effect

Table 2
The estimated charge based on various storage mechanism for as-prepared co-MnO_2.

Solution	q_T (C g^{-1})	q_0 (C g^{-1})	q_{TSM} (C g^{-1})	q_{SCM} (C g^{-1})	q_{DLC} (C g^{-1})	q_{SCM}/q_T (%)	q_{TSM}/q_T (%)	q_{DLC}/q_T (%)
0.1 M $Ba(NO_3)_2$	332.22	33.39	298.83	26.15–29.77	3.62–7.24	7.9–9.0	89.9	1.1–2.2
0.1 M KNO_3	165.29	31.12	134.17	24.34–27.73	3.39–6.78	14.7–16.8	81.2	2.0–4.1

q_{SCM}, q originated from the SCM; q_{TSM}, q originated from the TSM; q_{DLC}, q originated from the double-layer capacitance.

can store a small number of charges [1,28]. As the semiconducting material, the double layer capacitance per unit external surface area (C_{ext}) of MnO_2 is about 2–4 μF cm^{-2} [29,30], and q_{DLC} of co-MnO_2 is calculated according to the equation $q = CU = C_{ext}S_{BET}U$, as shown in Table 2. q_0 of co-MnO_2 are compose of q_{SCM} and q_{DLC}, and q_{SCM} is obtained. From Tables 1 and 2, q_{SCM} of co-MnO_2 is larger than that of Ba-MnO_2 and K-MnO_2. It may be inferred that the charges based on the SCM are related to the surface area, and the larger surface area may store more charges by the SCM. Regarding to the comprehensive relationship between the SCM and the surface area, there are few reports and we will study on it in the future. Table 2 shows the estimated charges based on various storage mechanism for as-prepared co-MnO_2 approximately. It shows that for as-prepared co-MnO_2, the charges based on the TSM accounted for 81.2–89.9% of the total charges and predominated; that the charges based on the SCM made up 7.9–16.8% and should not be negligible; and that the charged from the double-layer capacitance may be negligible (1.1–4.1%).

4. Conclusions

In order to investigate the co-existence of two mechanisms, the surface chemisorption mechanism and the tunnel storage mechanism, for the charge storage of MnO_2, the sample α-MnO_2 whose tunnels (2×2) were almost vacant was synthesized by chemical co-precipitation technique, and the sample Ba-MnO_2 and K-MnO_2 whose tunnels (2×2) were intercalated and stabilized with Ba^{2+} and K^+ were prepared by refluxing. By measuring the electrochemical characteristics, it can be inferred that for as-prepared co-MnO_2, both the TSM and SCM contribute to the charge storage and the TSM predominates within the total charges. For as-prepared Ba-MnO_2 and K-MnO_2, the charge storage basically depends on the SCM, as the cations (Ba^{2+} and K^+) occupying the tunnels in advance may block the cations of the electrolyte from intercalating into the tunnels and the charges cannot be stored by the TSM.

For as-prepared co-MnO_2, the contribution of TSM and SCM is estimated. The charges based on the TSM account for 81.2–89.9% of the total charges; the charges based on the SCM may contribute to 7.9–16.8% that are not be negligible; the charges from the double-layer capacitance contribute to only 1.1–4.1% of all the charges and may be negligible.

Acknowledgements

This work was financially supported by the Natural Science Foundation of China under Grants No. 50632040, 50802049 and 50902079, Fundamental Research Program of Shenzhen (Jc200903180520A). We also appreciate the financial support from Guangdong Province Innovation R&D Team Plan.

References

[1] P. Simon, Y. Gogotsi, Nat. Mater. 7 (2008) 845–854.
[2] C.J. Xu, F.Y. Kang, B.H. Li, H.D. Du, J. Mater. Res. 25 (2010) 1421–1432.
[3] A.G. Pandolfo, A.F. Hollenkamp, J. Power Sources 157 (2006) 11–27.
[4] D. Zhai, B. Li, F. Kang, Micropor. Mesopor. Mater. 130 (2010) 224–228.
[5] E. Naudin, H.A. Ho, L. Breau, D. Belanger, J. Phys. Chem. B 106 (2002) 10585–10593.
[6] B.E. Conway, V. Birss, J. Wojtowicz, J. Power Sources 66 (1997) 1–14.
[7] J.P. Zheng, Electrochem. Solid State Lett. 2 (1999) 359–361.
[8] H.Y. Lee, J.B. Goodenough, J. Solid State Chem. 144 (1999) 220–223.
[9] C.J. Xu, B.H. Li, H.D. Du, F.Y. Kang, Y.Q. Zeng, J. Power Sources 180 (2008) 664–670.
[10] O. Ghodbane, J.L. Pascal, F. Favier, ACS Appl. Mater. Int. 1 (2009) 1130–1139.
[11] T. Brousse, M. Toupin, R. Dugas, L. Athouel, O. Crosnier, D. Belanger, J. Electrochem. Soc. 153 (2006) A2171–A2180.
[12] R.N. Reddy, R.G. Reddy, J. Power Sources 132 (2004) 315–320.
[13] M. Toupin, T. Brousse, D. Belanger, Chem. Mater. 16 (2004) 3184–3190.
[14] S.L. Kuo, N.L. Wu, J. Electrochem. Soc. 153 (2006) A1317–A1324.
[15] Q.T. Qu, P. Zhang, S. Tian, Y.P. Wu, R. Holze, J. Phys. Chem. C 113 (2009) 14020–14027.
[16] V. Subramanian, H.W. Zhu, B.Q. Wei, J. Power Sources 159 (2006) 361–364.
[17] C.J. Xu, H.D. Du, B.H. Li, F.Y. Kang, Y.Q. Zeng, J. Electrochem. Soc. 156 (2009) A73–A78.
[18] Q. Feng, H. Kanoh, Y. Miyai, K. Ooi, Chem. Mater. 7 (1995) 148–153.
[19] M.H. Rossouw, D.C. Liles, S. Hull, Mater. Res. Bull. 27 (1992) 221–230.
[20] F. Qi, H. Kanoh, K. Ooi, M. Tani, Y. Nakacho, J. Electrochem. Soc. 141 (1994) L135–L136.
[21] J. Liu, V. Makwana, J. Cai, S.L. Sui, M. Aindow, J. Phys. Chem. B 107 (2003) 9185–9194.
[22] R.N. Deguzman, Y.F. Shen, E.J. Neth, S. Levine, J.M. Newsam, Chem. Mater. 6 (1994) 815–821.
[23] T. Ohzuku, M. Kitagawa, K. Sawai, T. Hirai, J. Electrochem. Soc. 138 (1991) 360–365.
[24] E.P. Barrett, L.G. Joyner, P.P. Halenda, J. Am. Chem. Soc. 73 (1951) 373–380.
[25] S. Ardizzone, G. Fregonara, S. Trasatti, Electrochim. Acta 35 (1990) 263–267.
[26] M. Toupin, T. Brousse, D. Belanger, Chem. Mater. 14 (2002) 3946–3952.
[27] A. Zolfaghari, F. Ataherian, M. Ghaemi, A. Gholami, Electrochim. Acta 52 (2007) 2806–2814.
[28] Y. Yang, Battery 36 (2006) 34–36.
[29] H. Shi, Electrochim. Acta 41 (1996) 1633–1639.
[30] J. Bockris, A. Reddy, Plenum Pub. Corp, New York, 1973.